

Motion-Refined DINOSAUR for Unsupervised Multi-Object Discovery

Xinrui Gong^{*1} Oliver Hahn^{*1} Christoph Reich^{1,2,3,4} Krishnakant Singh¹
 Simone Schaub-Meyer^{1,5} Daniel Cremers^{2,3,4} Stefan Roth^{1,4,5}
¹TU Darmstadt ²TU Munich ³MCML ⁴ELIZA ⁵hessian.AI ^{*}equal contribution
<https://github.com/visinf/mr-dinosaur>

Abstract

Unsupervised multi-object discovery (MOD) aims to detect and localize distinct object instances in visual scenes without any form of human supervision. Recent approaches leverage object-centric learning (OCL) and motion cues from video to identify individual objects. However, these approaches use supervision to generate pseudo labels to train the OCL model. We address this limitation with MR-DINOSAUR—Motion-Refined DINOSAUR—a minimalist unsupervised approach that extends the self-supervised pre-trained OCL model, DINOSAUR [56], to the task of unsupervised multi-object discovery. We generate high-quality unsupervised pseudo labels by retrieving video frames without camera motion for which we perform motion segmentation of unsupervised optical flow. We refine DINOSAUR’s slot representations using these pseudo labels and train a slot deactivation module to assign slots to foreground and background. Despite its conceptual simplicity, MR-DINOSAUR achieves strong multi-object discovery results on the TRI-PD and KITTI datasets, outperforming the previous state of the art despite being fully unsupervised.

1. Introduction

Achieving an instance-level understanding of complex scenes is a long-standing challenge in computer vision, with broad applications in autonomous driving, robotics, and medical image analysis [see 47, 75, for an overview]. Approaching instance-level scene understanding via supervised learning requires pixel-wise ground-truth labels [7, 11, 28, 40], yet obtaining large amounts of manual pixel-wise annotation is highly resource intensive. For instance, annotating a single 2 MP image of a natural scene can take even a trained human annotator up to multiple hours [8, 15]. Approaching instance-level scene understanding using unsupervised learning aims to overcome the challenges associated with human annotations. In our work, we specifically aim to detect and localize distinct object instances in visual

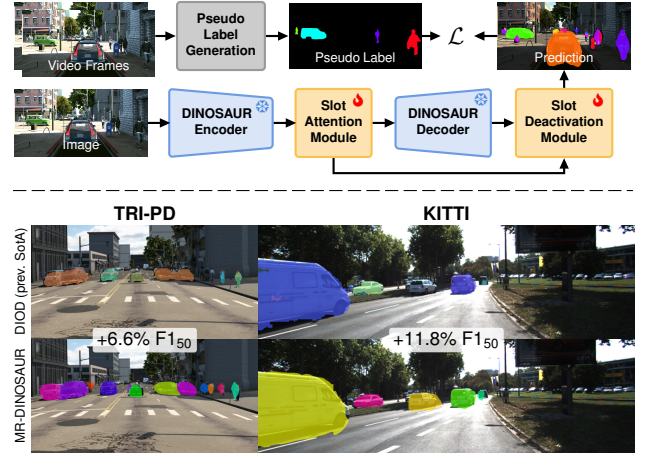


Figure 1. **Overview and results of our unsupervised multi-object discovery approach MR-DINOSAUR.** We propose a minimalist approach to generate instance pseudo-labels from motion for refining slot representations of the DINOSAUR model. Further, we train our proposed slot deactivation module to distinguish foreground from background slots (*top*). MR-DINOSAUR outperforms the previous SotA approach DIOD, indicated by the gains in $F1_{50}$ (*bottom*).

scenes without *any* form of human supervision. Hereby, objects are defined as entities capable of moving.

Object-centric learning (OCL) aims at compositional scene understanding by decomposing images into localized object representations using Slot Attention [46]. Trained using self-supervised objectives, recent slot attention-based methods [33, 56, 70] have been scaled to work on real-world images. Though slot-attention methods are able to successfully decompose a scene, using them for instance-level scene understanding remains challenging for two key reasons: *First*, slot-attention approaches specify a fixed number of slots and divide each image into an equal number of segments, including the background. Due to using the fixed number of segments, they suffer from poor segmentation of objects, such as over- and under-segmentation [76]. *Second*, identifying which slot is foreground and background is not trivial.

Bao *et al.* [4] were one of the first to apply slot-attention mechanisms successfully to instance-level scene understanding, which is commonly referred to as multi-object discovery [65] in the slot-attention literature. We, henceforth, adopt this terminology. Bao *et al.* [4] relies on synthetic video data [17] and supervised motion segmentation masks for learning foreground and background slots. Subsequent approaches built on [4] by improving the architecture [5], explicitly modeling the background segmentation [34], or mitigating noise in motion-based pseudo-labels via self-distillation [35]. Yet, these methods still entail significant limitations, such as requiring synthetic pre-training to perform well on real-world data and utilizing supervised pipelines for pseudo-label generation.

In this work, we pursue a highly minimalist take on unsupervised multi-object discovery. We propose MR-DINOSAUR—**M**otion **R**efined **D**INOSAUR—transferring DINOSAUR [56], a scalable object-centric learning approach, to the task of multi-object discovery (*cf.* Fig. 1). On its own, DINOSAUR, like other slot-attention methods, suffers from imprecise object masks and is unable to classify slots as either foreground or background. We address this by refining the slot representations and learning to distinguish foreground from background using a straightforward and strictly unsupervised motion guidance. By using video frames that entail no camera motion, we can cluster unsupervised optical flow to obtain high-quality instance pseudo-labels as flow is only induced by moving objects. Using these pseudo-labels, we propose a novel two-stage training scheme, and slot deactivation module, enabling MR-DINOSAUR to outperform existing methods for the task of multi-object discovery.

Specifically, we make the following contributions: (i) We obtain high-precision unsupervised instance pseudo-labels of real-world scenes by retrieving quasi-static frames (*i.e.*, frames with no camera motion) and straightforward motion clustering. (ii) We effectively extend DINOSAUR to the task of multi-object discovery by refining DINOSAUR’s predictions and adding a simple, yet effective slot deactivation module. (iii) Despite being minimalist and fully unsupervised, MR-DINOSAUR yields state-of-the-art unsupervised multi-object discovery accuracy on KITTI and TRI-PD.

2. Related Work

Object-centric learning (OCL) aims to decompose a complex visual scene into a set of semantically meaningful object representations. These representations can be used for compositional generation and downstream tasks such as property prediction [46], compositional generation [1, 29], and building world models [71]. Initial work [10, 23, 25, 30, 43–45] in OCL employed sequential architectures to decompose the input scene, but is hard to

scale to complex scenes and imposes an unnatural ordering on objects. To overcome these issues, [20, 21] proposed using stick-breaking priors, while [46] introduced a slot-attention (SA) mechanism, which uses the standard dot-product attention [64] and an iterative refinement scheme. Its ease of use and the scalability of dot-product attention have led to the widespread adoption of slot attention for OCL [4, 19, 39, 56].

Slot-attention methods for real-world scenes. Until recently, SA methods were trained in the pixel space, which limited their applicability to synthetic datasets [26, 32, 37]. DINOSAUR [56] scaled SA by leveraging features from self-supervised architectures such as DINO [13] and learning the slots/object-centric representation by reconstructing these semantic features instead of pixels. SPOT [33] improves DINOSAUR by utilizing student-teacher training. Parallel to these approaches, [1, 30, 58, 70] have used a diffusion-based decoder for scaling slot attention to real-world scenes. These methods focus on image reconstruction rather than scene decomposition. Despite the successes of DINOSAUR [56], existing SA methods need to specify the number of objects (slots) a-priori for each dataset. This limits these methods, leading to issues of over-segmentation and under-segmentation [76]. We address these issues by refining the slot representation using guidance from unsupervised motion masks and learning to classify each slot into foreground or background.

Guided multi-object discovery. Unsupervised object discovery for images is an ill-posed problem in the absence of a precise definition of an object. Utilizing video data alleviates this problem, as the principle of common fate [41] can be used to define what an object is. Most existing methods utilize additional signals such as depth [19], optical flow [36, 39], and motion segmentation [5]. However, relying on motion masks makes these methods over-segment the background and unable to segment static objects. BMOD [34] addressed the issue of over-segmenting the background by introducing and explicitly learning a background slot, guided using masks of moving objects. Another issue in using motion masks for guidance is that these masks are often noisy, making the guidance signal poor; DIOD [35] tackles this issue and extends BMOD with a self-distillation loss that better handles the noisy guidance masks. Compared to earlier works, we simply refine the DINOSAUR model with masks obtained from our novel motion-based pseudo-labeling. Once we refine the encoder model, we train a simple MLP to distinguish between foreground and background slots.

Optical flow-based motion segmentation aims to localize moving objects in imagery by exploiting optical flow [2, 73]. While some approaches only estimate a single foreground motion mask, others obtain object-wise masks [74]. Early approaches employed flow discontinu-

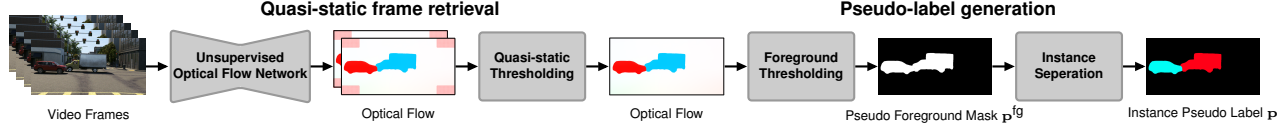


Figure 2. **Pseudo-label generation.** We derive pseudo-instance labels in two stages. First, we perform an unsupervised retrieval of quasi-static frames, *i.e.* those without camera motion, identified by SMURF [60] optical flow being small in most of the image corners. Given frames with quasi-static camera motion, we perform simplistic motion segmentation, where the foreground mask for moving objects arises by applying a threshold. Connected components and HDBSCAN clustering leads to our instance pseudo label for quasi-static frames.

ities [22, 55, 62], motion trajectories [9, 49], or probabilistic motion models [6, 59, 63]. Recent approaches learned to estimate motion segments using synthetic data with ground-truth masks [17], supervised foundation models [72], or self-supervised learning [14, 54]. We propose a simple yet precise motion segmentation approach by first retrieving video frames without camera motion. Fulfilling the static background assumption significantly simplifies the motion segmentation task.

3. MR-DINOSAUR

Our work approaches the problem of multi-object discovery, *i.e.*, segmenting all objects in a scene, where objects are defined as entities capable of moving. Our novel unsupervised multi-object discovery method is comprised of two stages. First, we generate high-quality unsupervised pseudo labels using motion cues (*cf.* Sec. 3.1). Second, we introduce a pseudo-label-based refinement strategy to extend the OCL method DINOSAUR [56] for multi-object discovery, overcoming its inability to distinguish between foreground and background—that is, between object and non-object regions. An overview of each part is provided in Figs. 2 and 3.

3.1. Pseudo-label generation

Our pseudo-label generation comprises two steps: (1) we retrieve quasi-static frames, *i.e.*, frames that do not entail camera motion from the training videos, and (2) pseudo instance-label generation, for which we employ a simple, yet effective motion segmentation approach on the optical flow of the quasi-static frames.

Quasi-static frames retrieval. We retrieve *quasi-static* frames, characterized by minimal camera motion, to generate accurate pseudo instance masks. In these frames, the static background ensures that optical flow predominantly arises from moving objects, allowing for simple clustering to do instance pseudo-labeling. Given two consecutive video frames $\mathbf{I}_1, \mathbf{I}_2 \in \mathbb{R}^{3 \times H \times W}$, we compute forward optical flow $\mathbf{f} \in \mathbb{R}^{2 \times H \times W}$ using the off-the-shelf *unsupervised* optical flow estimation approach SMURF [60]. To assess the amount of camera motion, we compute the average flow magnitude within each image corner region, denoted as $\|\mathbf{f}_i\|$, $i \in \{0, 1, 2, 3\}$. Since foreground objects typically appear near the image center, we exploit this scene

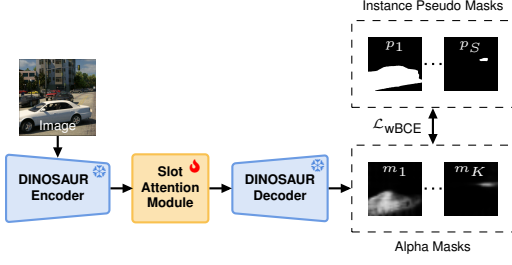
structure. We label frames as quasi-static if at least three of the four corner patches have average flow magnitudes below τ_{static} . In practice, these corner patches each cover 15% of the image height and width (Fig. 2). We find this simple approach to work surprisingly well (*e.g.*, 99% Accuracy on KITTI; *cf.* Tab. 7).

Pseudo-label generation. Equipped with quasi-static frames and their optical flow, we aim to obtain instance-wise pseudo masks. We propose a simple pseudo-label generation, depicted in Fig. 2. We first obtain a foreground mask and extract connected components. Subsequently, connected components that potentially comprise multiple objects are partitioned.

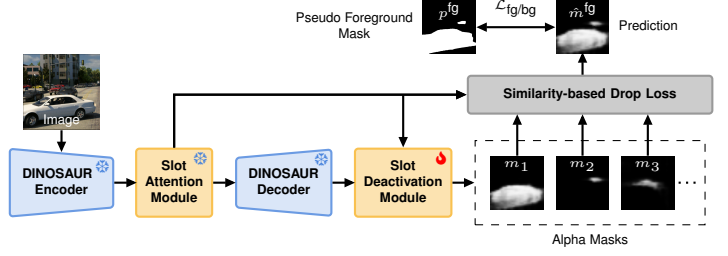
First, as quasi-static frames exhibit no camera motion, we simply derive a foreground mask by thresholding the estimated optical flow \mathbf{f} . In particular, we threshold the optical flow magnitude $\|\mathbf{f}_{:,h,w}\| > \tau_{\text{fg}}$, obtaining a binary foreground mask $\mathbf{p}^{\text{fg}} \in \{0, 1\}^{H \times W}$. To detect individual instances within the foreground mask \mathbf{p}^{fg} , we first extract the connected components [18], *i.e.*, all spatially disjoint segments. Still, connected components can include one or multiple objects due to overlapping objects. To separate multiple instances within a single connected component, we leverage the common fate principle—pixels with similar motion likely belong to the same object [69].

To identify connected components that potentially encapsulate multiple objects, we utilize the spatial derivatives of the estimated optical flow. Motion discontinuities signaled by large derivatives suggest that a connected component is composed of multiple objects. In particular, we threshold the norm of the gradient magnitudes $\|(\nabla f_{1,h,w}, \nabla f_{2,h,w})\| > \tau_{\nabla}$ for all points inside each connected component (*i.e.*, ignoring outside contours). If a connected component contains such a sudden change, we will further divide the segment, utilizing HDBSCAN clustering [12]. For each pixel in the connected component, we use the flow magnitude, flow angle, and its pixel position as an input feature for clustering. Our pseudo-label generation produces a variable number S of high-quality instance pseudo masks $\mathbf{p} \in \{0, 1\}^{S \times H \times W}$ per quasi-static frame.

Discussion. While there are more advanced motion segmentation approaches available [6, 16, 17, 27, 54, 59, 72], we aim for simplicity and rely on an unsupervised opti-



(a) MR-DINOSAUR training stage 1.



(b) MR-DINOSAUR training stage 2.

Figure 3. **MR-DINOSAUR architecture and training overview.** Stage 1 trains the DINOSAUR slot-attention module using our proposed pseudo-labels. DINOSAUR alpha masks are supervised with pseudo-label instance masks using a weighted binary cross-entropy loss. Stage 2 trains our slot deactivation module using $\mathcal{L}_{fg/bg}$ to learn to discriminate between foreground and background slots.

cal flow-based motion clustering approach for pseudo-label generation. Our approach is conceptually simple, captures non-rigid motions, and produces a *variable* number of pseudo-instance masks, accurately discovering foreground objects, albeit only for the subset of quasi-static frames.

3.2. Refining DINOSAUR

We aim to refine and extend DINOSAUR [56], an established unsupervised object-centric representation learning approach, to perform unsupervised multi-object discovery using our pseudo-instance masks. DINOSAUR decomposes an image into a set of regions, each binding to individual objects or distinct scene components, including the background. While our pseudo-instance masks only capture objects that are actually moving, they provide an informative cue to differentiate between foreground objects and background. To this end, we propose a novel two-stage training scheme. The first stage employs our pseudo-instance masks to enhance the accuracy of the predicted DINOSAUR slot masks. The second stage relies on a novel slot-deactivation module, which enables DINOSAUR to discriminate between foreground and background. Our two-stage training is illustrated in Fig. 3. We refer to the resulting model as motion-refined DINOSAUR, or MR-DINOSAUR for short.

DINOSAUR [56] learns a set of representations, decomposing an image into localized and semantically coherent regions. It encodes images with DINO [13, 50], followed by a slot-attention mechanism [46] to group the features into K slot vectors $\mathbf{z} \in \mathbb{R}^{K \times D_{\text{slots}}}$ via an iterative attention mechanism. Next, the slot representations are decoded utilizing an MLP. While a transformer decoder can be used as well, Seitzer *et al.* [56] found that this leads to slots binding more to semantic representations than objects. We hence use an MLP decoder. Consecutively, each slot representation is independently broadcast onto the image patches, and a learned positional encoding is added to each token. Each token is processed by the same MLP, yielding a feature reconstruction $\hat{\mathbf{y}}_k$ and map α_k that indicates the region

attended to by each slot. The final feature reconstruction is given by

$$\mathbf{y} = \sum_{k=1}^K \hat{\mathbf{y}}_k \odot \mathbf{m}_k, \quad \mathbf{m}_k = \text{softmax } \alpha_k, \quad (1)$$

where \odot denotes the element-wise multiplication. The training objective is to reconstruct the DINO features with \mathbf{y} . In the following, we refer to the softmax masks $\mathbf{m} \in \mathbb{R}^{K \times H \times W}$ as alpha masks. Our method builds upon a “vanilla” DINOSAUR model, trained on the respective dataset as proposed by [56], which is then refined and extended to the task of multi-object discovery by our method.

Stage 1: Taming the DINOSAUR. Equipped with the pseudo-instance labels from Sec. 3.1, we aim to refine DINOSAUR’s slot representations to better bind to objects. To that end, training stage 1 fine-tunes the predicted alpha masks $\mathbf{m} \in \mathbb{R}^{K \times H \times W}$ of the K slots using our pseudo labels \mathbf{p} . In particular, we match the alpha masks to the individual masks of the pseudo label using Hungarian matching [42]. We apply a weighted binary cross-entropy loss $\mathcal{L}_{\text{wBCE}}$ using the matched masks. In particular, $\mathcal{L}_{\text{wBCE}}$ between the $S \leq K$ matched predictions $\tilde{\mathbf{m}}_s$ and the respective pseudo instance mask \mathbf{p}_s for the slot s is defined as:

$$\mathcal{L}_{\text{wBCE}}(\tilde{\mathbf{m}}_s, \mathbf{p}_s) = \frac{1}{H \cdot W} \sum_{h,w} \left[(2 - r_s) \mathbf{p}_s \log \tilde{\mathbf{m}}_s + (1 - \mathbf{p}_s) \log(1 - \tilde{\mathbf{m}}_s) \right], \quad (2)$$

with weight $r_s = \frac{1}{H \cdot W} \sum_{h,w} \mathbf{p}_s$, which aids in detecting small objects. Specifically, if $r_s \rightarrow 0$ as the pseudo instance mask \mathbf{p}_s only includes a few pixels, then $(2 - r_s) \rightarrow 2$, up-weighting small-object masks in the loss. We train the slot-attention module while freezing the encoder and decoder. This first training stage already leads to improved slot representations, localizing objects (*cf.* Sec. 4).

Stage 2: Letting the DINOSAUR see objects. While DINOSAUR decomposes the entire image into slots, we extend it to perform unsupervised multi-object discovery by

learning to discriminate slots that encode foreground objects from slots encoding background. Given the refined DINOSAUR model after stage 1 training, we now aim to classify slots into foreground and background using our pseudo labels from Sec. 3.1 as the training signal. We strive for a minimalist approach and introduce a slot deactivation module ϕ_d , which predicts a weight vector $\lambda \in \mathbb{R}^K$ from the slot representations \mathbf{z} . The slot-deactivation module is an MLP with a final sigmoid layer predicting a weight λ close to 0 for background slots and close to 1 for foreground slots:

$$\lambda = \phi_d(\mathbf{z}), \quad (3)$$

where λ_k is the predicted probability of slot k being classified as foreground. For obtaining the foreground prediction \mathbf{m}^{fg} of the model, the alpha masks \mathbf{m}_k are simply weighted by the predicted λ_k . During inference, λ is binarized, *i.e.*, if $\lambda_k > 0.5$, the corresponding slot k is kept; otherwise, the slot k is deactivated, meaning its alpha mask \mathbf{m}_k is weighted with zero.

Drop-loss. In training stage 2, we train the proposed slot-deactivation module while keeping the entire DINOSAUR model frozen (Fig. 3b). The training is guided by our foreground pseudo-label mask \mathbf{p}^{fg} (*cf.* Sec. 3.1). However, we obtain pseudo-instance masks only for dynamic objects in a scene when captured by a quasi-static camera. This can lead to inconsistent training signals for the foreground/background separation if an object of the same category is static in another frame (*e.g.*, driving *vs.* parked cars) and, therefore, the corresponding slot representation would be considered once as foreground and once as background.

To allow our model to discover objects beyond the dynamic ones captured in our pseudo labels, we carefully select the relevant alpha mask predictions $\hat{\mathbf{m}}^{\text{fg}}$ to be considered in the loss computation and ignore predictions in the loss that might be correct (static objects) but are not part of the pseudo label (dynamic objects). Inspired by [66], we propose a similarity-based drop-loss mechanism, where we ignore a slot in our loss term if its alpha mask is not matched to any pseudo-instance mask, but its slot representation yields high cosine similarity to the representation of one of the matched slots. Specifically, after matching, we have S matched alpha mask predictions $\tilde{\mathbf{m}}_s$ and slot representations $\tilde{\mathbf{z}}_s$, as well as $U = K - S$ unmatched alpha mask predictions $\tilde{\mathbf{m}}_u$ and slot representations $\tilde{\mathbf{z}}_u$. We calculate the cosine similarity of each unmatched slot representation to all matched slot representations as $\mathbf{c}_u = \text{cos-sim}(\tilde{\mathbf{z}}_u, \tilde{\mathbf{z}}_s)$. When applying the similarity-based drop-loss mechanism, the foreground prediction $\hat{\mathbf{m}}^{\text{fg}}$ considered in the loss arises as follows. We consider all matched slots (dynamic objects) and all unmatched slots that are dissimilar to the matched slots (background):

$$\hat{\mathbf{m}}^{\text{fg}} = \sum_s \lambda_s \mathbf{m}_s + \sum_u \mathbb{1}(\max \mathbf{c}_u \leq \tau_{\text{drop}}) \lambda_u \mathbf{m}_u, \quad (4)$$

where τ_{drop} refers to the slot similarity threshold (*e.g.*, $\tau_{\text{drop}} = 0.99$).

Given $\hat{\mathbf{m}}^{\text{fg}}$ and the foreground pseudo-label \mathbf{p}^{fg} , we employ a foreground-background loss. This loss combines a negative log-likelihood (NLL) loss to learn the foreground and a background regularization term. Hereby, we prevent the model from collapsing to the trivial solution of predicting foreground for all pixels. The foreground-background loss is defined as

$$\mathcal{L}_{\text{fg/bg}}(\hat{\mathbf{m}}^{\text{fg}}, \mathbf{p}^{\text{fg}}) = \mathcal{L}_{\text{fg}}(\hat{\mathbf{m}}^{\text{fg}}, \mathbf{p}^{\text{fg}}) + \mathcal{L}_{\text{bg}}(\hat{\mathbf{m}}^{\text{fg}}, \mathbf{p}^{\text{fg}}), \quad (5)$$

where the foreground NLL loss is given as

$$\mathcal{L}_{\text{fg}}(\hat{\mathbf{m}}^{\text{fg}}, \mathbf{p}^{\text{fg}}) = \frac{1}{H \cdot W} \sum_{h,w} \mathbf{p}^{\text{fg}} \log \hat{\mathbf{m}}^{\text{fg}}. \quad (6)$$

Given the number of background pixels N_{bg}^{p} in the pseudo-label \mathbf{p}^{fg} , the background regularization component is defined as

$$\mathcal{L}_{\text{bg}}(\hat{\mathbf{m}}^{\text{fg}}, \mathbf{p}^{\text{fg}}) = \frac{r_{\text{bg}}}{N_{\text{bg}}^{\text{p}}} \sum_{h,w} \mathbb{1}(\mathbf{p}^{\text{fg}} = 0) \hat{\mathbf{m}}^{\text{fg}}. \quad (7)$$

4. Experiments

We compare MR-DINOSAUR against state-of-the-art slot-attention methods for video and image object discovery across multiple datasets, following the common evaluation protocol [4, 5, 34, 35]. We refer to the supplemental material for additional results.

Datasets. To train and evaluate, we use two datasets: First, TRI-PD [4], a synthetic dataset simulating driving scenarios. The training set comprises 924 photorealistic videos. Each video is 10 seconds long and captured at 20 FPS. 51 additional videos from disjoint scenes serve for evaluation. Second, KITTI [24], a real-world dataset capturing urban driving scenarios. We train on KITTI raw data and evaluate on the 200 images of the instance segmentation subset. We exclude the validation samples from the training data.

Metrics. We evaluate using $F1_{50}$, the harmonic mean of precision AP_{50} and recall AR_{50} at a mask IoU threshold of 50 %. $F1_{50}$ inherently normalizes object sizes and effectively penalizes background over-segmentation by treating each spurious background segment as a false positive. In addition, we use fg-ARI, a standard metric in object discovery that quantifies the similarity between predicted and ground-truth clusterings by computing the ARI only over foreground regions. In addition, we use all-ARI [34], which incorporates background regions in the ARI computation. However, the pixel-wise nature of ARI metrics inherently favors the accurate segmentation of larger objects, as correctly clustering many pixels disproportionately boosts the score. Note that recent papers have raised concerns regarding the reliability of the fg-ARI metric [21, 33, 37,

Table 1. **Unsupervised multi-object discovery on TRI-PD** using $F1_{50}$, AP_{50} , AR_{50} , all-ARI, and fg-ARI (all in %, \uparrow). * denotes methods using DINOv2. Underlined methods use supervision.

Method	$F1_{50}$	AP_{50}	AR_{50}	all-ARI	fg-ARI
SlotAttention [46] NeurIPS'20	–	–	–	–	10.2
MONet [10] arXiv'19	–	–	–	–	11.0
SCALOR [31] ICLR'20	–	–	–	–	18.6
IODINE [25] ICML'19	–	–	–	–	9.8
MCG [52] TPAMI'15	–	–	–	–	25.1
Bao <i>et al.</i> [4] CVPR'22	12.2	–	–	6.3	50.9
MoTok [5] CVPR'23	12.6	–	–	4.7	55.1
BMOD [34] WACV'24	14.4	–	–	28.6	53.9
BMOD* [34] WACV'24	16.3	–	–	29.1	58.5
DIOD [35] CVPR'24	35.4	28.9	45.6	70.3	66.1
DIOD* [35] CVPR'24	41.5	37.8	45.9	74.1	69.7
DINOSAUR* [56] ICLR'23	4.9	2.8	19.8	2.2	52.0
MR-DINOSAUR* (<i>Ours</i>)	48.1	45.1	51.5	71.9	74.4

48, 56, 70]. In particular, fg-ARI has been shown to be sensitive to segmentation biases, potentially favoring either over-segmentation [21, 48] or under-segmentation. In addition, excluding background pixels from the evaluation may not fully capture object segmentation performance [37, 48]. ARI results must thus be considered with caution.

Baseline. We utilize DINOSAUR [56] and follow the training and inference setup proposed by Seitzer *et al.* [56]. Hereby, inference on non-square images is performed using a non-overlapping sliding window approach with square image crops. To address objects spanning across multiple windows being segmented by multiple masks, we incorporate the slot merger mechanism [3] for evaluation. Specifically, masks located at the borders of the sliding window crops are merged utilizing agglomerative clustering based on the cosine similarity of the slot representations.

Implementation details. We use PyTorch [51] and build upon the code of DINOSAUR [56], SMURF [60], and DIOD [35]. For pseudo-label generation, we apply a quasi-static frame retrieval threshold of $\tau_{\text{static}} = 0.5$ for TRI-PD and $\tau_{\text{static}} = 1.7$ for KITTI. We use a foreground mask threshold of $\tau_{\text{fg}} = 2.5$, and an inner mask flow-gradient threshold of $\tau_{\nabla} = 20$. We utilize the DINOSAUR framework to train the baseline models with DINOv2 [50] encoder using 60 slots in total per image. Specifically, we use 2×30 slots for TRI-PD and 4×15 slots for KITTI. The background loss weight r_{bg} is set to 0.2, the similarity-based drop loss uses $\tau_{\text{drop}} = 0.99$. The slot-deactivation module is a four-layer MLP with a hidden dimension of 2048 and a sigmoid activation for the last layer. Following previous work [4, 5, 34, 35], we resize and crop images to a resolution of 980×490 for TRI-PD and 1260×378 for KITTI for both pseudo-labeling and training. Training is performed on two non-overlapping square crops of size 490 for TRI-PD and four overlapping crops of size 378 for KITTI. Stage 1 trains for 15 epochs using a learning rate of $4e-6$. In

Table 2. **Unsupervised multi-object discovery on KITTI** using $F1_{50}$, AP_{50} , AR_{50} , all-ARI, and fg-ARI (all in %, \uparrow). * denotes methods using DINOv2, \dagger methods pre-trained on synthetic TRI-PD data, and \ddagger re-training on KITTI only, for a fair comparison. Underlined methods use supervision.

Method	$F1_{50}$	AP_{50}	AR_{50}	all-ARI	fg-ARI
SlotAttention [46] NeurIPS'20	–	–	–	–	13.8
MONet [10] arXiv'19	–	–	–	–	14.9
SCALOR [31] ICLR'20	–	–	–	–	21.1
IODINE [25] ICML'19	–	–	–	–	14.4
MCG [52] TPAMI'15	–	–	–	–	40.9
STEVE [57] NeurIPS'22	–	–	–	–	11.9
SAVI [39] ICLR'21	–	–	–	–	20.0
PPMP [36] NeurIPS'22	–	–	–	–	51.9
SAVI++ [19] NeurIPS'22	–	–	–	–	23.9
Bao <i>et al.</i> \dagger [4] CVPR'22	8.8	–	–	4.2	47.1
MoTok \dagger [5] CVPR'23	8.2	–	–	2.1	64.4
BMOD \dagger [34] WACV'24	9.3	–	–	17.8	54.7
BMOD* \dagger [34] WACV'24	10.9	–	–	21.7	60.8
DIOD \dagger [35] CVPR'24	18.0	17.6	18.4	61.6	73.5
DIOD* \dagger [35] CVPR'24	23.2	26.3	20.8	81.6	72.3
DIOD* \ddagger [35] CVPR'24	14.1	14.4	13.8	27.7	52.6
DINOSAUR* [56] ICLR'23	5.7	3.6	13.7	1.1	72.0
MR-DINOSAUR* (<i>Ours</i>)	35.0	59.7	24.7	74.9	74.1

stage 2, training is performed for one epoch using a learning rate of $4e-5$. We use a batch size of 8 and optimize with Adam [38]. All experiments use a *single* NVIDIA A6000 Ada GPU. We refer to the supplement for more details.

4.1. Comparison to the state of the art

The most competitive methods, following the same task setup as we do, include Bao *et al.* [4], BMOD [34], and DIOD [35]. Since these methods use the same pseudo-labels [4] generated with the supervised motion segmentation approach TSAM [17], all methods implicitly use some form of supervision and cannot be considered completely unsupervised. In contrast, our approach MR-DINOSAUR is *fully* unsupervised. An additional limitation of prior work when applied to real-world images is the reliance on pre-training with synthetic images. First, we compare our method against recent work on the synthetic TRI-PD dataset in Tab. 1. MR-DINOSAUR outperforms competing approaches across all metrics, except for all-ARI, where we score slightly lower. In particular, our method improves $F1_{50}$ by 6.6% points over the state-of-the-art DIOD [35]. Regarding the ARI metrics, we would like to refer to Sec. 4 summarizing the concerns of previous works [21, 33, 37, 48, 56, 70] and shift the focus to the established $F1_{50}$. While BMOD [34] and DIOD [35] incorporate temporal information from multiple frames during both training and inference on TRI-PD, we use video frame pairs solely for pseudo-label generation. Second, Tab. 2, we compare against prior work on the KITTI dataset. MR-DINOSAUR outperforms the previous approaches across fg-ARI, $F1_{50}$,

Table 3. **Analyzing MR-DINOSAUR** training stage contribution (a), drop loss contribution (b), and number of available slots (c). We report F1₅₀, all-ARI, fg-ARI (all in %, ↑) trained and evaluated on the TRI-PD dataset.

(a) Training analysis.				(b) Drop loss analysis.				(c) Number of slots analysis.			
Method	F1 ₅₀	all-ARI	fg-ARI	Method	F1 ₅₀	all-ARI	fg-ARI	Num. Slots	F1 ₅₀	all-ARI	fg-ARI
DINOSAUR*[56]	4.9	2.2	52.0	DINOSAUR*[56]	4.9	2.2	52.0	40	45.9	69.2	73.9
+ Stage 1	12.5	3.3	75.6	Ours w/o drop loss	46.3	70.5	73.3	60	48.1	71.9	74.4
+ Stage 2	48.1	71.9	74.4	Ours w/ drop loss	48.1	71.9	74.4	80	43.8	67.6	70.2
+ Only Stage 2	25.9	68.8	50.9								

AP₅₀, and AR₅₀. We perform slightly worse in terms of the all-ARI metric. Outperforming the state of the art on the challenging F1₅₀ metric is a significant result given that MR-DINOSAUR does not use any form of supervision. For comparison on equal footing, we trained the current state-of-the-art approach DIOD on the real-world KITTI data only, without pre-training on TRI-PD (cf. Tab. 2; DIOD*[†]). This leads to a severe drop in DIOD’s results despite using the same DINOv2 features as our approach. MR-DINOSAUR improves 11.8 % points over the state-of-the-art DIOD [35] and 20.9 % points over DIOD trained only on KITTI in terms of F1₅₀.

4.2. Analyzing MR-DINOSAUR

We analyze the individual components of MR-DINOSAUR through several ablation experiments.

Architecture analysis. In Tab. 3, we analyze the impact of our architectural decisions and components. We find that both training stages boost multi-object discovery metrics (cf. Tab. 3a). Stage 1 refines the slot representations to bind objects more effectively, while stage 2 learns foreground segmentation, which increases the F1 score. Training only stage 2 for foreground-background distinction is possible, but leads to significantly worse results. In Tab. 3b, we train MR-DINOSAUR with and without our proposed similarity-based drop loss. We find that the drop loss enables the slot deactivation module to explore objects beyond the moving instances in the pseudo-labels. Finally, we examine different numbers of slots in Tab. 3c. While 60 slots yield a slight performance advantage, using 40 or 80 slots also produces good results.

Pseudo-label analysis. We evaluate our pseudo-labels both quantitatively and qualitatively. In Tab. 4, we analyze our pseudo-labels and compare them with the TSAM pseudo-labels introduced by Bao *et al.* [4] and adopted in recent works [5, 34, 35]. Our pseudo-labels differ fundamentally from TSAM labels. While TSAM provides a pseudo-label for every video frame—which introduces challenges for motion segmentation when the camera is moving—our approach generates pseudo-labels only for quasi-static frames. We compare TSAM and our pseudo-labels using both unsupervised SMURF [60] flow predictions used across all main experiments, and supervised RAFT [61] flow predictions. We evaluate the subset of images pseudo-

Table 4. **MR-DINOSAUR pseudo-label analysis** using F1₅₀, all-ARI, fg-ARI (all in %, ↑) on the TRI-PD dataset.

Method	# Samples	F1 ₅₀	all-ARI	fg-ARI
TSAM [4]	93729	8.9	18.1	20.2
TSAM [4]	12514	7.1	20.8	18.4
Ours	12514	15.4	32.9	41.5
Ours (w/ RAFT [61])	12514	15.1	34.1	41.1

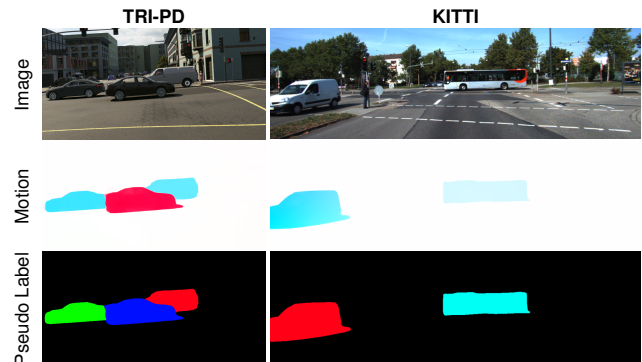


Figure 4. **Qualitative examples of our proposed pseudo-labels** on the TRI-PD [4] and KITTI [24] dataset.

Table 5. **MR-DINOSAUR with RAFT pseudo-labels.** We report F1₅₀, all-ARI, and fg-ARI (all in %, ↑) on the TRI-PD dataset.

Method	Pseudo Labels	F1 ₅₀	all-ARI	fg-ARI
DINOSAUR* [56]	–	4.9	2.2	52.0
MR-DINOSAUR* (Ours)	SMURF	48.1	71.9	74.4
MR-DINOSAUR* (Ours)	RAFT	50.8	74.7	74.9

labeled by our approach. Due to differences in motion prediction, the image sets for SMURF and RAFT pseudo-labels differ slightly. We restrict the evaluation to the 95 % shared samples. Our method outperforms the TSAM labels by a large margin. This is a significant result given that TSAM uses supervised training compared to our minimalistic unsupervised pseudo-labeling approach. Figure 4 shows qualitative results of our pseudo-labels for both KITTI and TRI-PD. We observe that our pseudo-instance masks exhibit high quality and precisely align with the contours of the moving objects. In Tab. 5, we train our method using pseudo-labels generated with RAFT. This yields comparable fg-ARI values and improvements in all-ARI and

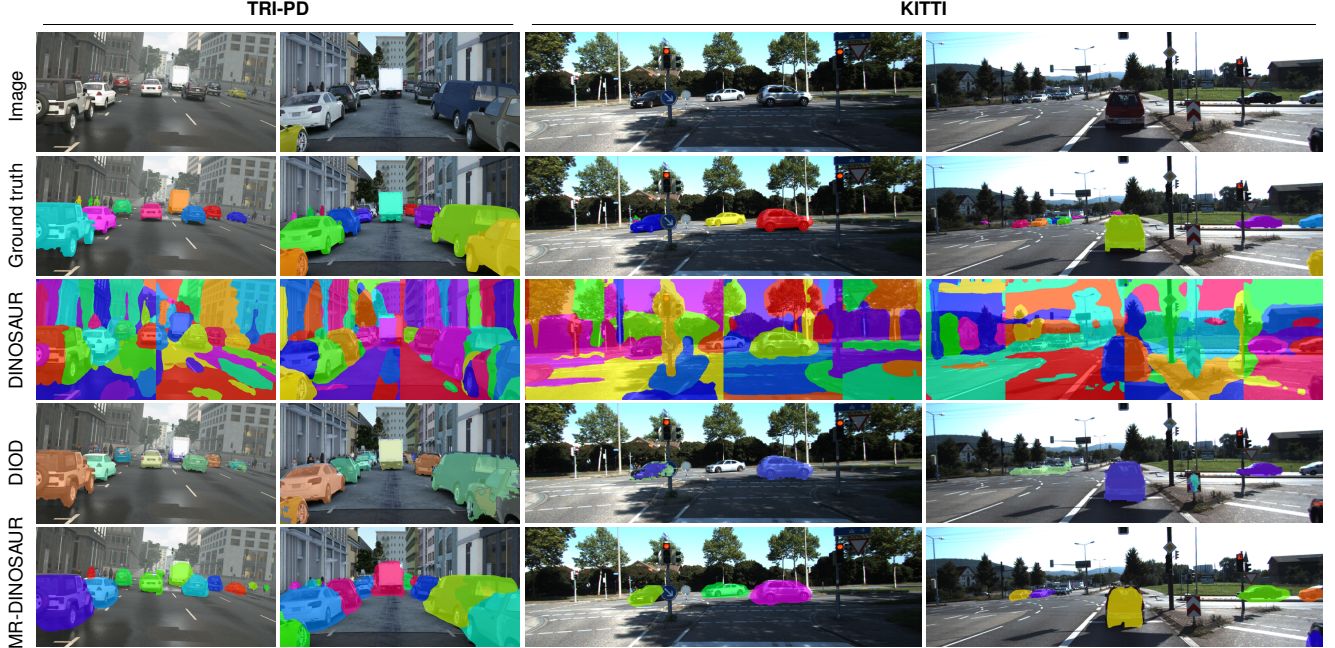


Figure 5. **Qualitative comparison** of our baseline DINOSAUR [56], DIOD [35], and MR-DINOSAUR (*Ours*) on the TRI-PD [4] and KITTI [24] datasets. We use random colors for different objects.

F1₅₀. Notably, using supervised RAFT flow, as done by DIOD, leads to state-of-the-art results on the all-ARI metric as well.

4.3. Qualitative results

We show qualitative results of our method MR-DINOSAUR and the baselines on both TRI-PD and KITTI datasets in Fig. 5. Compared to DIOD [35], we observe that MR-DINOSAUR leads to less noisy predictions, discovering a large number of objects while rarely predicting masks on the image background. MR-DINOSAUR predicts coarser masks compared to DIOD, which we attribute to the nature of the DINOSAUR slots. We discover more instances compared to DIOD, even for finely resolved distant objects.

5. Limitations and Future Work

Our pseudo-labels result from the static background assumption in our motion segmentation method. We rely on retrieving quasi-static frames and require training data captured with a static camera—a condition met in most but not all real-world scenarios. Additionally, using unsupervised flow estimation introduces apparent motion artifacts (*e.g.*, a car’s shadow in Fig. 4) in the pseudo-labels. More generally, current motion-based multi-object discovery approaches share a limitation: learning the concept of an object from motion is, by definition, restricted to object categories capable of moving [14, 35, 54]. In contrast, a related line of research [66–68] leverages pseudo-labels from the object-centricity of datasets (*e.g.*, ImageNet [53]) to learn

instances without supervision. Combining these strengths could offer a more comprehensive solution for multi-object discovery. In general, our method is agnostic to the baseline OCL approach, and could benefit from future, more advanced OCL approaches. In summary, we propose a minimalistic, fully unsupervised method for multi-object discovery that can be a foundation for advancing instance-level understanding.

6. Conclusion

We presented MR-DINOSAUR, extending the established OCL approach DINOSAUR for the task of unsupervised multi-object discovery. We demonstrate that selecting quasi-static video frames enables the generation of high-quality instance pseudo-labels without any supervision, as it simplifies the problem to clustering optical flow of moving objects. We effectively refined DINOSAUR using the proposed pseudo-labels and extended DINOSAUR for multi-object discovery by introducing a slot deactivation module to distinguish between foreground and background slots. We propose a unified framework for unsupervised multi-object discovery that requires less data, no supervision, and still achieves strong results across multiple benchmarks compared to previous approaches.

Acknowledgments. This project has received funding from the ERC under the European Union’s Horizon 2020 research and innovation programme (grant agreement No. 866008). This work has further been co-funded by the LOEWE initiative (Hesse, Germany) within the emergenCITY center [LOEWE/1/12/519/03/05.001(0016)/72] and the Deutsche Forschungsgemeinschaft (German Research Foundation, DFG) under Germany’s Excellence Strategy (EXC 3066/1 “The Adaptive Mind”, Project No. 533717223). This project was also partially supported by the European Research Council (ERC) Advanced Grant SIMULACRON, DFG project CR 250/26-1 “4D-YouTube”, and GNI Project “AICC”. Christoph Reich is supported by the Konrad Zuse School of Excellence in Learning and Intelligent Systems (ELIZA) through the DAAD programme Konrad Zuse Schools of Excellence in Artificial Intelligence, sponsored by the Federal Ministry of Education and Research. Finally, we acknowledge the support of the European Laboratory for Learning and Intelligent Systems (ELLIS). Special thanks go to Divyam Sheth for his last-minute help with the paper.

References

- [1] Adil Kaan Akan and Yucel Yemez. Slot-guided adaptation of pre-trained diffusion models for object-centric learning and compositional generation. In *ICLR*, 2025. 2
- [2] Shivangi Anthwal and Dinesh Ganotra. An overview of optical flow-based approaches for motion segmentation. *Imaging Sci. J.*, 67(5):284–294, 2019. 2
- [3] Gökay Aydemir, Weidi Xie, and Fatma Güney. Self-supervised object-centric learning for videos. In *NeurIPS*2023*, pages 32879–32899. 6, i, iii
- [4] Zhipeng Bao, Pavel Tokmakov, Allan Jabri, Yu-Xiong Wang, Adrien Gaidon, and Martial Hebert. Discovering objects that can move. In *CVPR*, pages 11779–11788, 2022. 2, 5, 6, 7, 8, ii, iii
- [5] Zhipeng Bao, Pavel Tokmakov, Yu-Xiong Wang, Adrien Gaidon, and Martial Hebert. Object discovery from motion-guided tokens. In *CVPR*, pages 22972–22981, 2023. 2, 5, 6, 7, i, iii
- [6] Michael J. Black and David J. Fleet. Probabilistic detection and tracking of motion boundaries. *Int. J. Comput. Vis.*, 38(3):231–245, 2000. 3
- [7] Daniel Bolya, Chong Zhou, Fanyi Xiao, and Yong Jae Lee. YOLACT: Real-time instance segmentation. In *ICCV*, pages 9156–9165, 2019. 1
- [8] Tim Brödermann, David Brüggemann, Christos Sakaridis, Kevin Ta, Odysseas Liagouris, Jason Corkill, and Luc Van Gool. MUSES: The multi-sensor semantic perception dataset for driving under uncertainty. In *ECCV*, pages 21–38, 2024. 1
- [9] Thomas Brox and Jitendra Malik. Object segmentation by long term analysis of point trajectories. In *ECCV*, pages 282–295, 2010. 3
- [10] Christopher P Burgess, Loic Matthey, Nicholas Watters, Rishabh Kabra, Irina Higgins, Matt Botvinick, and Alexander Lerchner. MONet: Unsupervised scene decomposition and representation. *arXiv:1901.11390 [cs.CV]*, 2019. 2, 6
- [11] Zhaowei Cai and Nuno Vasconcelos. Cascade R-CNN: High quality object detection and instance segmentation. *IEEE Trans. Pattern Anal. Mach. Intell.*, 43(5):1483–1498, 2019. 1
- [12] Ricardo J. G. B. Campello, Davoud Moulavi, and Jörg Sander. Density-based clustering based on hierarchical density estimates. In *PAKDD*, pages 160–172, 2013. 3
- [13] Mathilde Caron, Hugo Touvron, Ishan Misra, Hervé Jégou, Julien Mairal, Piotr Bojanowski, and Armand Joulin. Emerging properties in self-supervised vision transformers. In *ICCV*, pages 9650–9660, 2021. 2, 4
- [14] Subhabrata Choudhury, Laurynas Karazija, Iro Laina, Andrea Vedaldi, and Christian Rupprecht. Guess what moves: Unsupervised video and image segmentation by anticipating motion. In *BMVC*, page 554, 2022. 3, 8, i
- [15] Marius Cordts, Mohamed Omran, Sebastian Ramos, Timo Scharwächter, Markus Enzweiler, Rodrigo Benenson, Uwe Franke, Stefan Roth, and Bernt Schiele. The Cityscapes dataset for semantic urban scene understanding. In *CVPR*, pages 3213–3223. 1
- [16] Daniel Cremers and Stefano Soatto. Motion competition: A variational approach to piecewise parametric motion segmentation. *Int. J. Comput. Vis.*, 62(3):249–265, 2005. 3
- [17] Achal Dave, Pavel Tokmakov, and Deva Ramanan. Towards segmenting anything that moves. In *ICCVW*, pages 1493–1502, 2019. 2, 3, 6
- [18] Luigi Di Stefano and Andrea Bulgarelli. A simple and efficient connected components labeling algorithm. In *ICIAP*, pages 322–327, 1999. 3
- [19] Gamaleldin Elsayed, Aravindh Mahendran, Sjoerd Van Steenkiste, Klaus Greff, Michael C. Mozer, and Thomas Kipf. SAVi++: Towards end-to-end object-centric learning from real-world videos. In *NeurIPS*2022*, pages 28940–28954. 2, 6
- [20] Martin Engelcke, Oiwi Parker Jones, and Ingmar Posner. Genesis-v2: Inferring unordered object representations without iterative refinement. In *NeurIPS*2021*, pages 8085–8094. 2
- [21] Martin Engelcke, Adam R. Kosiorek, Oiwi Parker Jones, and Ingmar Posner. GENESIS: Generative scene inference and sampling with object-centric latent representations. In *ICLR*, 2020. 2, 5, 6
- [22] Wilfried Enkelmann. Obstacle detection by evaluation of optical flow fields from image sequences. *Image Vis. Comput.*, 9(3):160–168, 1991. 3
- [23] S. M. Ali Eslami, Nicolas Heess, Theophane Weber, Yuval Tassa, David Szepesvari, Koray Kavukcuoglu, and Geoffrey E Hinton. Attend, infer, repeat: Fast scene understanding with generative models. In *NIPS*2016*. 2
- [24] Andreas Geiger, Philip Lenz, Christoph Stiller, and Raquel Urtasun. Vision meets robotics: The KITTI dataset. *Int. J. Robot. Res.*, pages 1231–1237, 2013. 5, 7, 8, ii, iii
- [25] Klaus Greff, Raphaël Lopez Kaufman, Rishabh Kabra, Nick Watters, Christopher Burgess, Daniel Zoran, Loic Matthey, Matthew Botvinick, and Alexander Lerchner. Multi-object representation learning with iterative variational inference. In *ICML*, pages 2424–2433, 2019. 2, 6

- [26] Oliver Groth, Fabian B. Fuchs, Ingmar Posner, and Andrea Vedaldi. ShapeStacks: Learning vision-based physical intuition for generalised object stacking. In *ECCV*, pages 702–717, 2018. 2
- [27] Oliver Hahn, Christoph Reich, Nikita Araslanov, Daniel Cremers, Christian Rupprecht, and Stefan Roth. Scene-centric unsupervised panoptic segmentation. In *CVPR*, pages 24485–24495, 2025. 3
- [28] Kaiming He, Georgia Gkioxari, Piotr Dollár, and Ross B. Girshick. Mask R-CNN. *IEEE Trans. Pattern Anal. Mach. Intell.*, 42(2):386–397, 2020. 1
- [29] Jindong Jiang, Fei Deng, Gautam Singh, and Sungjin Ahn. Object-centric slot diffusion. In *NeurIPS*2023*, pages 8563–8601. 2
- [30] Jindong Jiang, Sepehr Janghorbani, Gerard De Melo, and Sungjin Ahn. Scalor: Generative world models with scalable object representations. In *ICLR*, 2019. 2
- [31] Jindong Jiang, Sepehr Janghorbani, Gerard de Melo, and Sungjin Ahn. SCALOR: Generative world models with scalable object representations. In *ICLR*, 2020. 6
- [32] Justin Johnson, Bharath Hariharan, Laurens Van Der Maaten, Li Fei-Fei, C. Lawrence Zitnick, and Ross Girshick. CLEVR: A diagnostic dataset for compositional language and elementary visual reasoning. In *CVPR*, pages 2901–2910, 2017. 2
- [33] Ioannis Kakogeorgiou, Spyros Gidaris, Konstantinos Karantzas, and Nikos Komodakis. SPOT: Self-training with patch-order permutation for object-centric learning with autoregressive transformers. In *CVPR*, pages 22776–22786, 2024. 1, 2, 5, 6, i
- [34] Sandra Kara, Hejer Ammar, Florian Chabot, and Quoc-Cuong Pham. The background also matters: Background-aware motion-guided objects discovery. In *WACV*, pages 1205–1214, 2024. 2, 5, 6, 7, iii
- [35] Sandra Kara, Hejer Ammar, Julien Denize, Florian Chabot, and Quoc-Cuong Pham. DIOD: Self-distillation meets object discovery. In *CVPR*, pages 3975–3985, 2024. 2, 5, 6, 7, 8, i, ii, iii
- [36] Laurynas Karazija, Subhabrata Choudhury, Iro Laina, Christian Rupprecht, and Andrea Vedaldi. Unsupervised Multi-object Segmentation by Predicting Probable Motion Patterns. In *NeurIPS*2022*, pages 2128–2141. 2, 6, i
- [37] Laurynas Karazija, Iro Laina, and Christian Rupprecht. Clevrtex: A texture-rich benchmark for unsupervised multi object segmentation. In *NeurIPS Datasets and Benchmarks*, 2021. 2, 5, 6
- [38] Diederik P. Kingma and Jimmy Ba. Adam: A method for stochastic optimization. In *ICLR*, 2015. 6
- [39] Thomas Kipf, Gamaleldin F. Elsayed, Aravindh Mahendran, Austin Stone, Sara Sabour, Georg Heigold, Rico Jonschkowski, Alexey Dosovitskiy, and Klaus Greff. Conditional object-centric learning from video. In *ICLR*, 2021. 2, 6
- [40] Alexander Kirillov, Eric Mintun, Nikhila Ravi, Hanzi Mao, Chloe Rolland, Laura Gustafson, Tete Xiao, Spencer Whitehead, Alexander C. Berg, Wan-Yen Lo, Piotr Dollár, and Ross Girshick. Segment anything. In *ICCV*, pages 4015–4026, 2023. 1
- [41] Kurt Koffka. Perception: An introduction to the gestalt-theorie. *Psychological Bulletin*, page 531, 1922. 2
- [42] Harold W. Kuhn. The Hungarian method for the assignment problem. *Nav. Res. Logist.*, 2(1-2):83–97, 1955. 4
- [43] Nanbo Li, Cian Eastwood, and Robert Fisher. Learning object-centric representations of multi-object scenes from multiple views. In *NeurIPS*2020*, pages 5656–5666. 2
- [44] Zhixuan Lin, Yi-Fu Wu, Skand Peri, Bofeng Fu, Jindong Jiang, and Sungjin Ahn. Improving generative imagination in object-centric world models. In *ICML*, pages 6140–6149, 2020.
- [45] Zhixuan Lin, Yi-Fu Wu, Skand Vishwanath Peri, Weihao Sun, Gautam Singh, Fei Deng, Jindong Jiang, and Sungjin Ahn. Space: Unsupervised object-oriented scene representation via spatial attention and decomposition. In *ICLR*, 2020. 2
- [46] Francesco Locatello, Dirk Weissenborn, Thomas Unterthiner, Aravindh Mahendran, Georg Heigold, Jakob Uszkoreit, Alexey Dosovitskiy, and Thomas Kipf. Object-centric learning with slot attention. In *NeurIPS*2020*, pages 11525–11538. 1, 2, 4, 6
- [47] Shervin Minaee, Yuri Boykov, Fatih Porikli, Antonio Plaza, Nasser Kehtarnavaz, and Demetri Terzopoulos. Image segmentation using deep learning: A survey. *IEEE Trans. Pattern Anal. Mach. Intell.*, 44(7):3523–3542, 2022. 1
- [48] Tom Monnier, Elliot Vincent, Jean Ponce, and Mathieu Aubry. Unsupervised layered image decomposition into object prototypes. In *ICCV*, pages 8620–8630, 2021. 6
- [49] Peter Ochs and Thomas Brox. Higher order motion models and spectral clustering. In *CVPR*, pages 614–621, 2012. 3
- [50] Maxime Oquab, Timothée Darcet, Théo Moutakanni, Huy V. Vo, Marc Szafraniec, Vasil Khalidov, Pierre Fernandez, Daniel Haziza, Francisco Massa, Alaaeldin El-Nouby, Mido Assran, Nicolas Ballas, Wojciech Galuba, Russell Howes, Po-Yao Huang, Shang-Wen Li, Ishan Misra, Michael Rabbat, Vasu Sharma, Gabriel Synnaeve, Hu Xu, Hervé Jégou, Julien Mairal, Patrick Labatut, Armand Joulin, and Piotr Bojanowski. DINOv2: Learning robust visual features without supervision. *Trans. Mach. Learn. Res.*, 2024. 4, 6
- [51] Adam Paszke, Sam Gross, Francisco Massa, Adam Lerer, James Bradbury, Gregory Chanan, Trevor Killeen, Zeming Lin, Natalia Gimelshein, Luca Antiga, Alban Desmaison, Andreas Köpf, Edward Yang, Zach DeVito, Martin Raison, Alykhan Tejani, Sasank Chilamkurthy, Benoit Steiner, Lu Fang, Junjie Bai, and Soumith Chintala. PyTorch: An imperative style, high-performance deep learning library. In *NeurIPS*2019*, pages 8024–8035. 6
- [52] Jordi Pont-Tuset, Pablo Arbeláez, Jonathan T. Barron, Ferran Marqués, and Jitendra Malik. Multiscale combinatorial grouping for image segmentation and object proposal generation. In *IEEE Trans. Pattern Anal. Mach. Intell.*, pages 128–140, 2015. 6
- [53] Olga Russakovsky, Jia Deng, Hao Su, Jonathan Krause, Sanjeev Satheesh, Sean Ma, Zhiheng Huang, Andrej Karpathy, Aditya Khosla, Michael S. Bernstein, Alexander C. Berg, and Li Fei-Fei. Imagenet large scale visual recognition challenge. *Int. J. Comput. Vis.*, 115(3):211–252, 2015. 8

- [54] Sadra Safadoust and Fatma Güney. Multi-object discovery by low-dimensional object motion. In *ICCV*, pages 734–744, 2023. 3, 8, i, iii
- [55] B. G. Schunck. Image flow segmentation and estimation by constraint line clustering. *IEEE Trans. Pattern Anal. Mach. Intell.*, 11(10):1010–1027, 1989. 3
- [56] Maximilian Seitzer, Max Horn, Andrii Zadaianchuk, Dominik Zietlow, Tianjun Xiao, Carl-Johann Simon-Gabriel, Tong He, Zheng Zhang, Bernhard Schölkopf, Thomas Brox, and Francesco Locatello. Bridging the gap to real-world object-centric learning. In *ICLR*, 2023. 1, 2, 3, 4, 6, 7, 8, i, ii, iii
- [57] Gautam Singh, Yi-Fu Wu, and Sungjin Ahn. Simple unsupervised object-centric learning for complex and naturalistic videos. In *NeurIPS*2022*, pages 18181–18196. 6
- [58] Krishnakant Singh, Simone Schaub-Meyer, and Stefan Roth. Guided latent slot diffusion for object-centric learning. *arXiv:2407.17929 [cs.CV]*, 2024. 2
- [59] Leonhard Sommer, Philipp Schröppel, and Thomas Brox. SF2SE3: Clustering scene flow into SE(3)-motions via proposal and selection. In *GCPR*, pages 215–229, 2022. 3
- [60] Austin Stone, Daniel Maurer, Alper Ayvaci, Anelia Angelova, and Rico Jonschkowski. SMURF: Self-teaching multi-frame unsupervised RAFT with full-image warping. *CVPR*, pages 3886–3895, 2021. 3, 6, 7, i
- [61] Zachary Teed and Jia Deng. RAFT: Recurrent all-pairs field transforms for optical flow. In *ECCV*, pages 402–419, 2020. 7
- [62] William B. Thompson, Kathleen M Mutch, and Valdis A Berzins. Dynamic occlusion analysis in optical flow fields. *IEEE Trans. Pattern Anal. Mach. Intell.*, 7(4):374–383, 1985. 3
- [63] Philip Torr. Geometric motion segmentation and model selection. *Philos. Trans. R. Soc. A*, 356(1740):1321–1340, 1998. 3
- [64] Ashish Vaswani, Noam Shazeer, Niki Parmar, Jakob Uszkoreit, Llion Jones, Aidan N. Gomez, Łukasz Kaiser, and Illia Polosukhin. Attention is all you need. In *NIPS*2017*. 2
- [65] José-Fabian Villa-Vásquez and Marco Pedersoli. Unsupervised object discovery: A comprehensive survey and unified taxonomy. *arXiv:2411.00868 [cs.CV]*, 2024. 2
- [66] Xudong Wang, Rohit Girdhar, Stella X. Yu, and Ishan Misra. Cut and learn for unsupervised object detection and instance segmentation. In *CVPR*, pages 3124–3134, 2023. 5, 8
- [67] Xudong Wang, Ishan Misra, Ziyun Zeng, Rohit Girdhar, and Trevor Darrell. Videocutler: Surprisingly simple unsupervised video instance segmentation. In *CVPR*, pages 22755–22764, 2024.
- [68] Yangtao Wang, Xi Shen, Yuan Yuan, Yuming Du, Maomao Li, Shell Xu Hu, James L. Crowley, and Dominique Vaufreydaz. Tokencut: Segmenting objects in images and videos with self-supervised transformer and normalized cut. *IEEE Trans. Pattern Anal. Mach. Intell.*, 45(12):15790–15801, 2023. 8
- [69] Max Wertheimer. Experimentelle studien über das sehen von bewegung. *Leipzig: J.A. Barth.*, 1912. 3
- [70] Ziyi Wu, Jingyu Hu, Wuyue Lu, Igor Gilitschenski, and Animesh Garg. SlotDiffusion: Object-centric generative modeling with diffusion models. In *NeurIPS*2023*, pages 50932–50958. 1, 2, 6
- [71] Ziyi Wu, Nikita Dvornik, Klaus Greff, Thomas Kipf, and Animesh Garg. Slotformer: Unsupervised visual dynamics simulation with object-centric models. In *ICLR*, 2023. 2
- [72] Junyu Xie, Charig Yang, Weidi Xie, and Andrew Zisserman. Moving object segmentation: All you need is SAM (and flow). In *ACCV*, pages 162–178, 2024. 3
- [73] Luca Zappella, Xavier Lladó, and Joaquim Salvi. Motion segmentation: A review. *Artif. Intell. Res. Dev.*, 184:398–407, 2008. 2
- [74] Dengsheng Zhang and Guojun Lu. Segmentation of moving objects in image sequence: A review. *Circuits, Syst. Signal Process.*, 20:143–183, 2001. 2
- [75] Tianfei Zhou, Fei Zhang, Boyu Chang, Wenguan Wang, Ye Yuan, Ender Konukoglu, and Daniel Cremers. Image segmentation in foundation model era: A survey. *arXiv:2408.12957 [CV.cv]*, 2024. 1
- [76] Roland S. Zimmermann, Sjoerd van Steenkiste, Mehdi S. M. Sajjadi, Thomas Kipf, and Klaus Greff. Sensitivity of slot-based object-centric models to their number of slots. *arXiv:2305.18890 [cs.CV]*, 2023. 1, 2

Motion-Refined DINOSAUR for Unsupervised Multi-Object Discovery

Supplementary Material

We first extend our approach to the synthetic multi-object video dataset MOVI-E [78]. Next, we evaluate the effectiveness of our quasi-static frames retrieval method used for pseudo-label generation. Additionally, we provide qualitative insights into our work, including failure cases, pseudo-label visualization, and MR-DINOSAUR results. We finish with details about the datasets employed, as well as the implementation details, to facilitate reproducibility.

A. MR-DINOSAUR on MOVI-E

We experiment on MOVI-E to broaden the range of datasets and methods for comparison. Because none of those methods report F1 or all-ARI on MOVI-E, we restrict our evaluation to fg-ARI here. MOVI-E [78] introduces a constant, artificial camera motion that violates our static-frame assumption for pseudo-labeling. Despite this disadvantage, our method achieves promising results in the ballpark of methods that explicitly deal with camera motion in the training data as shown in Tab. 6.

B. Quasi-static Frame Retrieval Analysis

We evaluate the effectiveness of our quasi-static frame retrieval method on the KITTI dataset, which includes detailed annotations of ground truth camera velocity for every video frame. Given that our motion segmentation approach used for pseudo-label generation relies on the static background assumption, the quasi-static frame retrieval plays an important role in achieving high-quality pseudo labels. We evaluate the quasi-static frame retrieval by comparing the set of frames our method retrieves from the training data to the ground-truth quasi-static frames. Ground-truth quasi-static frames are defined as frames with camera velocities below 0.2 m/s. Our method achieves an impressive 99.4 % accuracy, 99.2 % precision, and 96.6 % recall as shown in Tab. 7, confirming that thresholding the average flow magnitude at the image corners is a simple and effective way to retrieve quasi-static frames.

C. More Qualitative Results

We provide additional qualitative visualizations of our pseudo-labels and our proposed method MR-DINOSAUR, as well as failure cases.

C.1. Qualitative pseudo-label examples

Fig. 6 shows additional visualizations of our pseudo-labels comparing to TSAM pseudo labels. Consistent with the

Table 6. **Unsupervised multi-object discovery on MOVI-E** using fg-ARI. * denotes using DINOv2. Underlined methods use supervision.

Method	fg-ARI
<u>GWM</u> [14] BMVC’22	42.5
<u>SPOT</u> [33] CVPR’24	59.9
<u>PPMP</u> [36] NeurIPS’22	63.1
<u>DINOSAUR</u> [56] ICLR’23	65.1
<u>MoTok</u> [5] CVPR’23	66.7
Safadoust et al. [54] ICCV’23	78.3
VideoSAUR [79] NeurIPS’23	78.4
SOLV* [3] NeurIPS’23	80.8
DIOD* [35] CVPR’24	82.2
DINOSAUR* [56] ICLR’23	66.2
MR-DINOSAUR* (<i>Ours</i>)	80.1

Table 7. **Quasi-static frame retrieval analysis** using accuracy, precision, recall (all in %) on the KITTI dataset. We compare the set of frames retrieved from the training videos by our method to the set of frames with a ground-truth velocity smaller than 0.2 m/s.

Ground-truth Velocity	Accuracy	Precision	Recall
< 0.2 m/s	99.4	99.2	96.6

analysis in Sec. 4.2, our pseudo-labels are precise and of high quality for both synthetic TRI-PD and real-world KITTI data. Although some samples exhibit motion artifacts introduced by the unsupervised optical flow from SMURF [60] (e.g., the left KITTI image), we mainly observe accurate object masks. Compared to TSAM pseudo labels, our pseudo labels exhibit fewer artifacts.

C.2. Failure cases

We visualize representative failure cases for MR-DINOSAUR in Fig. 7. Occasionally, predictions cover non-object structures (e.g., a tree in the left image) and over-segmentation occurs on large objects with intricate textures (e.g., the truck in the right TRI-PD image). Precise segmentation of small, overlapping objects also remains challenging. Notably, similar issues—such as artifacts and missed small objects—are observed with the state-of-the-art DIOD [35] method.

C.3. Qualitative MR-DINOSAUR examples

Finally, Fig. 8 presents additional qualitative examples comparing our method, MR-DINOSAUR, to the baseline DINOSAUR [56] and DIOD [35]. While DINOSAUR establishes a solid foundation, it tends to undersegment and blur the distinction between objects and background. DIOD produces good qualitative results but often yields noisy

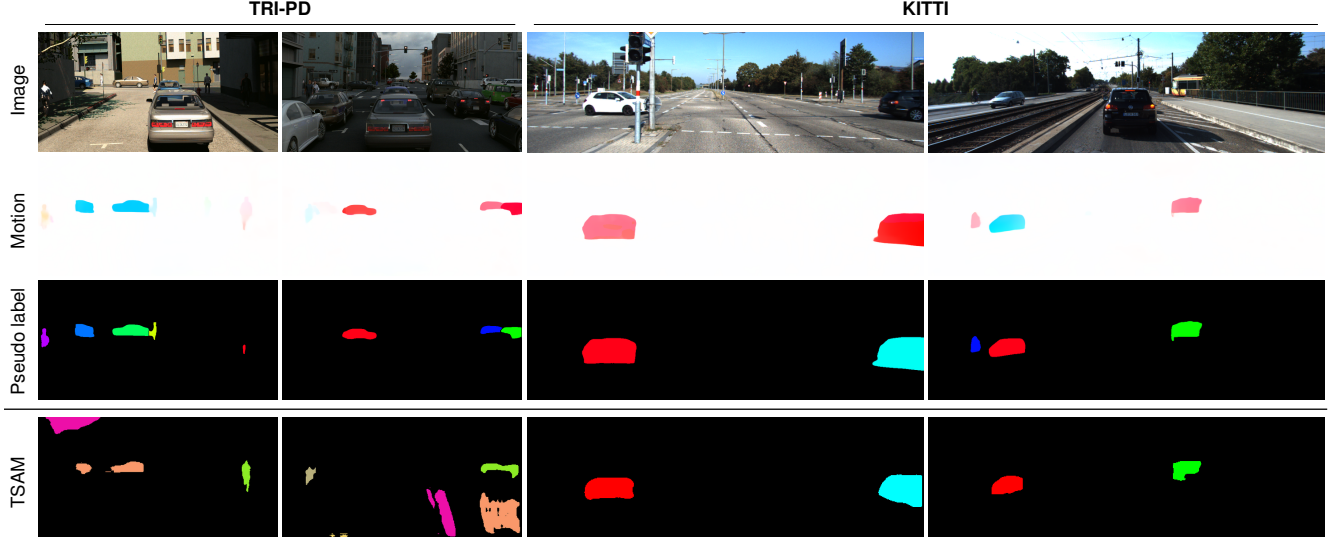


Figure 6. **Additional visualizations** of our pseudo-labels on the TRI-PD [4] and KITTI [24] dataset. We further visualize the respective TSAM pseudo labels used by DIOD [35]. Here we use random colors for different objects.

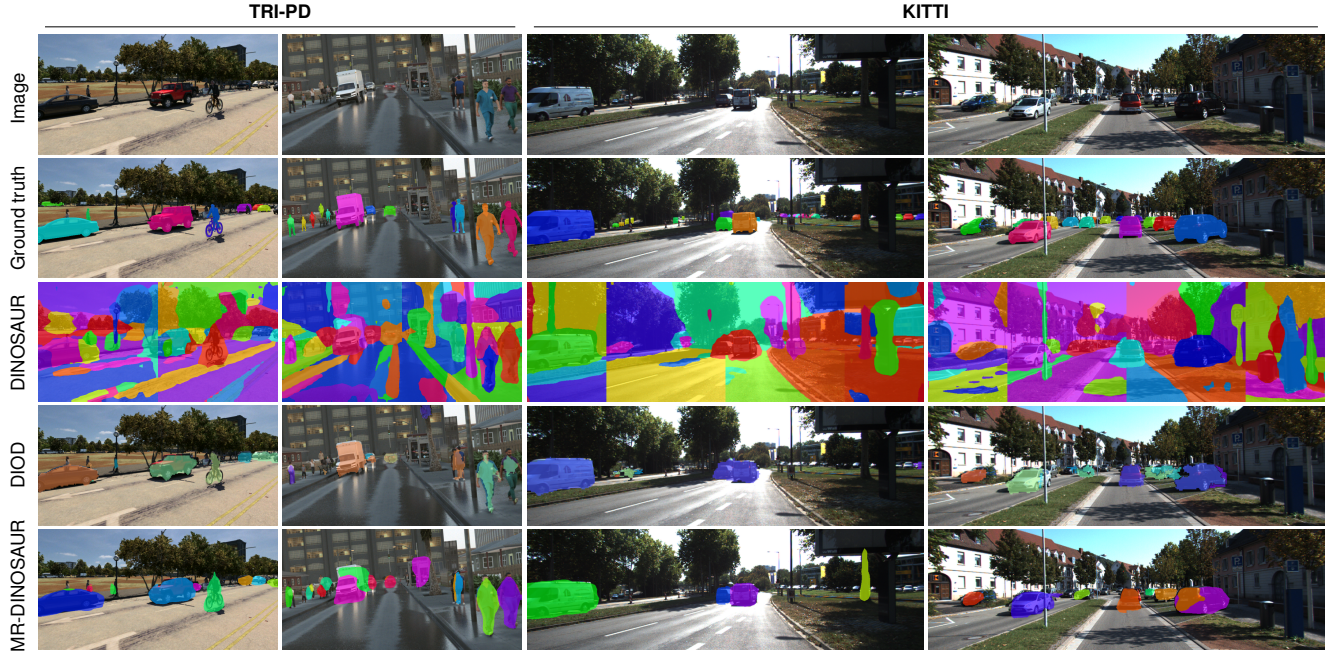


Figure 7. **Failure cases** of MR-DINOSAUR (*Ours*) comparing to DIOD [35] and our baseline DINOSAUR [56] on the TRI-PD [4] and KITTI [24] dataset. Here we use random colors for different objects.

masks by merging multiple objects into a single mask or missing objects entirely. In contrast, MR-DINOSAUR effectively differentiates foreground from background, resulting in fewer false positives and demonstrating superior capability in detecting small instances.

D. Reproducibility

To facilitate reproducibility, we elaborate on the technical and implementation details. Note that our code is available at <https://github.com/visinf/mrdinosaur>.

D.1. Datasets

TRI-PD [4] is a synthetic urban driving-scene dataset extracted from Parallel Domain [77]. It includes detailed

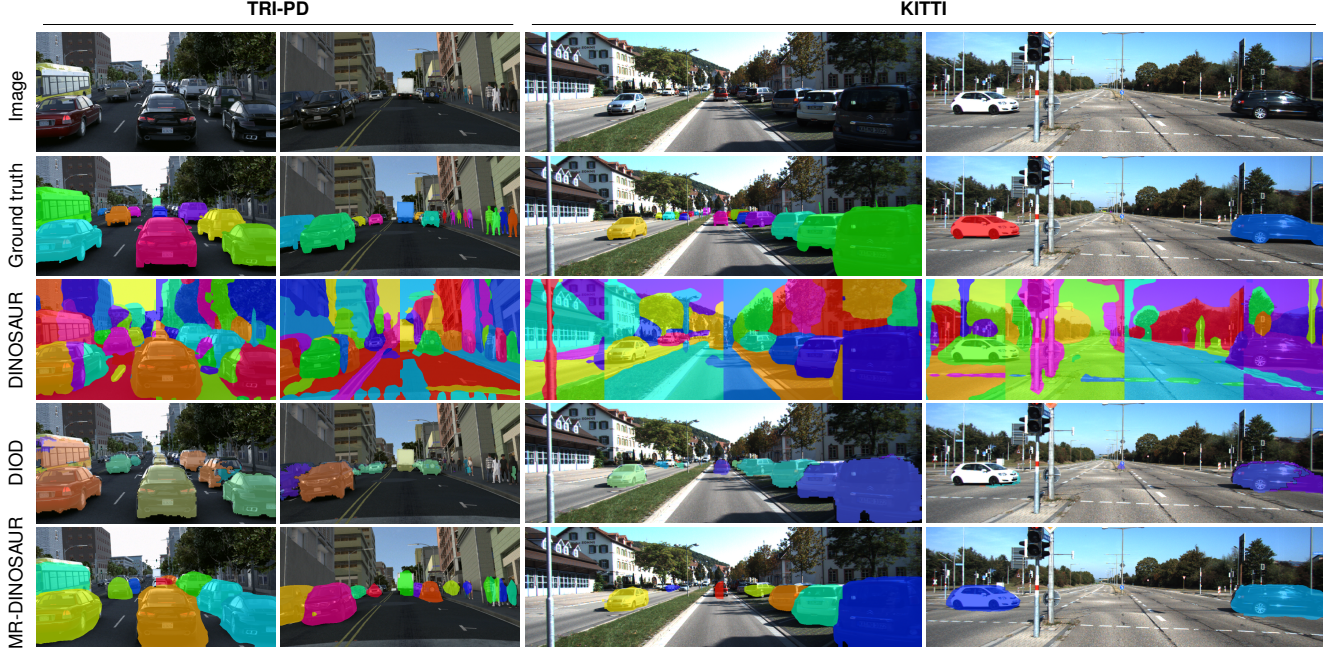


Figure 8. **Qualitative comparison** of our baseline DINOSAUR [56], DIOD [35], and MR-DINOSAUR (*Ours*) on the TRI-PD [4] datasets and KITTI [24]. Here we use random colors for different object instances.

annotations, including camera pose, calibration, depth, instance segmentation, semantic segmentation, 2D/3D bounding box, depth, forward/backward 2D motion vectors, and forward/backward 3D motion vectors. The training set consists of 200 photorealistic scenes captured by six cameras, each with 200 frames; the validation set comprises 17 scenes recorded by three cameras, totaling 10 200 frames. In this paper, we only use the three front-camera frames that align with the validation set for training. Following previous work [4, 5, 34, 35], we discard scenarios with low visibility (*e.g.*, foggy and dark scenes), resulting in 157 scenes and a total of 94 200 frames, for training DINOSAUR. From these, we extract 13 280 quasi-static frames for training MR-DINOSAUR. The resolution of all frames is 1216×1936 . Following previous work [4, 5, 34, 35], we resize and crop the images to a resolution of 980×490 for pseudo-labeling and training. Training is performed on two non-overlapping square crops of size 490×490 .

KITTI [24] is a widely used autonomous driving dataset. It includes various sensor data collected from various environments, *e.g.*, urban, rural, and highway scenes, offering extensive annotations and a diverse range of scenarios. We train DINOSAUR using all images provided in the raw data, resulting in 95 778 frames from 151 videos. We retrieve 12 526 quasi-static frames for training MR-DINOSAUR. For evaluation, we utilize the instance segmentation subset, which consists of 200 frames with a res-

olution of 375×1242 . Each frame is an individual image, rather than part of a consecutive sequence. Also, following previous work [4, 5, 34, 35], we resize the images to a resolution of 378×1260 for pseudo-labeling and training. Training is performed on four non-overlapping square crops of size 378×378 .

MOVI [78] is a synthetic video dataset comprising six sub-datasets (MOVI-A to MOVI-F) of increasing complexity. Each sub-dataset consists of generated scenes, with each scene representing a two-second rigid-body simulation of falling objects. The sub-datasets vary in object count and type, background, camera trajectory, and whether all objects are in motion or some remain stationary. We experiment on the MOVi-E dataset used by several previous works on multi-object discovery [3, 5, 35, 54, 79]. MOVi-E introduces simple camera movement, where the camera moves along a straight line at a random but constant velocity. Each video consists of 24 frames, with the training set containing 9749 videos (a total of 233 976 frames) and the validation set containing 250 videos (a total of 6000 frames). We randomly selected 9 frames from each video for training, resulting in a total of 87 741 images used for training DINOSAUR. We retrieve 84 831 quasi-static frames for training MR-DINOSAUR. Images originally at 256×256 are resized to 266×266 for training to account for the patch size of DINOv2.

Table 8. DINOSAUR and MR-DINOSAUR hyperparameters used for the results on the TRI-PD, KITTI, and MOVI-E datasets.

DINOSAUR				
Dataset		TRI-PD	KITTI	MOVI-E
Training steps		500k	500k	500k
Batch size		16	64	64
Optimizer		Adam	Adam	Adam
Number of warmup steps		10k	10k	10k
Peak learning rate		1e-4	4e-4	4e-4
Exponential decay half-life		100k	100k	100k
ViT architecture		DINOv2-ViT-B/14	DINOv2-ViT-B/14	DINOv2-ViT-B/14
Image/Crop size		490	378	266
Cropping strategy		Random	Random	Full
Augmentations		Random Horizontal Flip	Random Horizontal Flip	-
Decoder	Type	MLP	MLP	MLP
	Layers	4	4	4
	MLP hidden dimension	2048	2048	1024
Slot Attention	Number of slots	30	15	24
	Total number of slots	60	60	24
	Iterations	3	3	3
	Slot dimension D_{slots}	32	32	128
MR-DINOSAUR				
Pseudo label generation	Quasi-static frame retrieval threshold τ_{static}	0.5	1.7	1.7
	Foreground mask threshold τ_{fg}	2.5	2.5	2.5
	Flow-gradient threshold τ_{∇}	20	20	20
Training stage 1	Training epochs	15	15	15
	Batch size	8	8	8
	Learning rate	4e-06	4e-06	4e-06
Training stage 2	Training epochs	1	1	1
	Batch size	8	8	8
	Learning rate	4e-05	4e-05	4e-05
	Regularization term α	0.2	0.2	0.2
	Drop similarity τ_{drop}	0.99	0.99	0.99
Slot deactivation module	Layers	4	4	4
	MLP hidden dimension	2048	2048	2048

D.2. Computational Requirements

All experiments use a single NVIDIA RTX 6000 Ada Generation GPU (48 GB VRAM) in a workstation equipped with an AMD EPYC 7343 CPU (32 cores) and 512 GB RAM.

On TRI-PD, a full 500 000-step training of the DINOSAUR baseline takes approximately 267 h, involving 97.3 M parameters, of which 10.7 M are trainable. For MR-DINOSAUR, training stage 1 (15 epochs, batch size 8) takes approximately 11 h, utilizing the same 97.3 M parameters, of which 634 K are trainable. Training stage 2 (1 epoch, batch size 8) takes approximately 40 min and utilizes 105.8 M parameters with 8.5 M trainable. Peak memory usage reaches 40.2 GB. At inference, we process an image at a resolution of 490×980 in 740 ms.

D.3. Further Implementation Details

Finally, we provide an overview of all hyperparameters used for training the baseline DINOSAUR and our method MR-DINOSAUR in Tab. 8.

References

- [77] Parallel Domain. <https://paralleldomain.com/>. June 2025. [ii](#)
- [78] Klaus Greff, Francois Belletti, Lucas Beyer, Carl Doversch, Yilun Du, Daniel Duckworth, David J. Fleet, Dan Gnanaprasam, Florian Golemo, Charles Herrmann, Thomas Kipf, Abhijit Kundu, Dmitry Lagun, Issam H. Laradji, Hsueh-Ti Derek Liu, Henning Meyer, Yishu Miao, Derek Nowrouzezahrai, A. Cengiz Öztireli, Etienne Pot, Noha Radwan, Daniel Rebain, Sara Sabour, Mehdi S. M. Sajjadi, Matan Sela, Vincent Sitzmann, Austin Stone, Deqing Sun, Suhani Vora, Ziyu Wang, Tianhao Wu, Kwang Moo Yi, Fangcheng Zhong and Andrea Tagliasacchi. Kubric: A scalable dataset generator. In *CVPR*, pages 3739–3751, 2022. [i](#), [iii](#)
- [79] Andrii Zadaianchuk, Maximilian Seitzer, and Georg Martius. Object-centric learning for real-world videos by predicting temporal feature similarities. In *NeurIPS*2023*. [i](#), [iii](#)